ACS Macro Letters

Letter

pubs.acs.org/macroletters

One-Step Production of Anisotropically Etched Graphene Using Supercritical Water

Takaaki Tomai,* Naoki Tamura, and Itaru Honma*

Institute of Multidisciplinary Research for Advanced Materials, Tohoku University, 2-1-1, Katahira, Aoba-ku, Sendai 980-8577, Japan

Supporting Information

ABSTRACT: We developed a one-step method for production of anisotropically etched graphene using supercritical fluid (SCF). Anisotropic etching of a graphite substrate and dispersed graphite powder with Ag nanoparticles was conducted in supercritical water (SCW). Because of the exfoliation effect of SCF, graphene was isolated from the graphite simultaneously with the anisotropic etching. High-resolution transmission electron microscopy (HRTEM) and Raman spectroscopy revealed the production of multilayer graphene exfoliated from the anisotropically etched graphite surface.

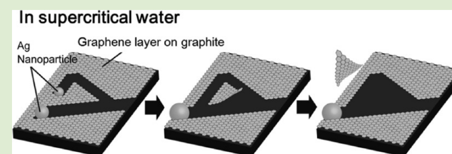

Unlike an ideal graphene with large sheet size, the characteristics of finite-sized graphene sheets are strongly affected by the edge type such as armchair and zigzag.[1] Control of graphene edge types has attracted considerable attention as a promising approach to manipulating the characteristics of graphene. For example, nonbonding π-electrons in the zigzag edge region are responsible for unconventional magnetic properties.[2−4] In the case of the application to electrochemical devices, which requires a large mass of graphene, it has been reported that the usage of the nanometer-sized graphene with abundant edge enhances the performance of electrochemical devices such as a lithium battery,[5,6] a supercapacitor,[7] and fuel cells.[8,9] However, due to the lack of techniques for the efficient production of graphene with controlled edges, it is poorly understood which type of edge is effective.

Recently, crystallographic etching of graphene/graphite has been discussed because of its high potential for precise control of the graphene edge.[10−15] Armchair and zigzag edges of graphene have different reactivities[16,17] and energetic stabilities.[18] It has been reported that because of the difference of reactivity to catalysts the selective introduction of zigzag edges can be achieved through catalytic etching. Etching of graphene/graphite by various metal and metal oxide particles has been observed under oxygen,[13,14,19,20] carbon dioxide, water,[20−22] and hydrogen[10,11,15] gaseous environments, where etch channels were formed by the catalyst.

The channeling mechanism in crystallographic etching in an oxidative environment is suggested to proceed as follows:[13] Catalytic nanoparticles deposited on the graphite tend to attach at surface defects like step edges. At elevated temperatures, the oxidizing agents, such as oxygen molecules, adsorbed on the catalytic particles release atomic oxygen. Atomic oxygen diffuses toward the graphene edge in the particle and reacts with carbon atoms in contact with the particle. Carbon atoms located at the graphene edges are more susceptible to oxidation than atoms within the bottom graphene sheet and thus become oxidized first. The gaseous products of the reaction (CO, CO_2) desorb, and the particle follows the receding graphene edge. Thus, the particle effectively channels a trench in the graphene layers. The direction of the channeling is anisotropic because of the anisotropy of the interaction of the catalyst particles with the crystalline graphene layers.

Although crystallographic etching is the most promising method for the precise control of the graphene edges on substrates, an extra peeling process of the etched graphene layers from the surface is required for the production of graphene with controlled edges. Moreover, in conventional crystallographic etching under a gaseous environment, the treated area is limited to the surface of the substrate or aggregated particles, and it is difficult to treat a large amount of dispersed graphite particles.

Therefore, in this study, we conducted anisotropic etching of a graphite surface in supercritical water (SCW), which is high density and high temperature water and enables us to treat the dispersed graphite powder. Via the exfoliation effect of supercritical fluid (SCF) simultaneously with the anisotropic etching, we succeeded in one-step production of anisotropically etched graphene. Moreover, we applied this method not only to a graphite substrate but also to graphite powder and confirmed the introduction of zigzag edges to dispersed graphite particles in the fluid.

In our experiment, Ag nanoparticles (Φ20−40 nm, QSI-Nano Silver, QuantumSphere, Inc.) were dispersed in 5 mL of ethanol at a concentration of 0.02 mg/mL. Ag is known to act as a catalyst for the etching reaction under oxidative environments.[13,14,19] We attached the Ag nanoparticles to a freshly cleaved surface of the highly oriented pyrolytic graphite (HOPG) substrate (10 mm × 5 mm) using a dip-drawing method and dried the substrate in a vacuum oven at 70 °C.

Etching in SCW (critical point of water: 374 °C, 22 MPa) was carried out by placing 2 mL of ultrapure water (Millipore, Q-grade) and the Ag-supported HOPG substrate into a batch-type Hastelloy reactor with a 10 mL capacity. In the reactor, 8

Received: April 16, 2013
Accepted: August 19, 2013
Published: August 21, 2013

ACS Publications © 2013 American Chemical Society

mL of gaseous ambient air containing approximately 7×10^{-5} mol of oxygen was also included. SCW is completely miscible with oxygen and the other gases created by the etching reaction. The reactor was placed in a specially designed furnace for 10 min. After the SCW treatment with oxygen, the reactor was removed from the furnace and immersed in a water bath to stop the reaction. Similar to the previous report on the temperature dependency of the oxidative catalytic etching of graphene by Ag nanoparticles, the etching reaction in this system showed large temperature dependency (see Supporting Information Figure S1). Below the temperature of 450 °C, the etching reaction had hardly been observed. Therefore, in this study, we set the temperature of the furnace to be 500 °C.

Figure 1(a) and (b) shows a scanning electron microscope (SEM) image of the HOPG surface before and after the etching

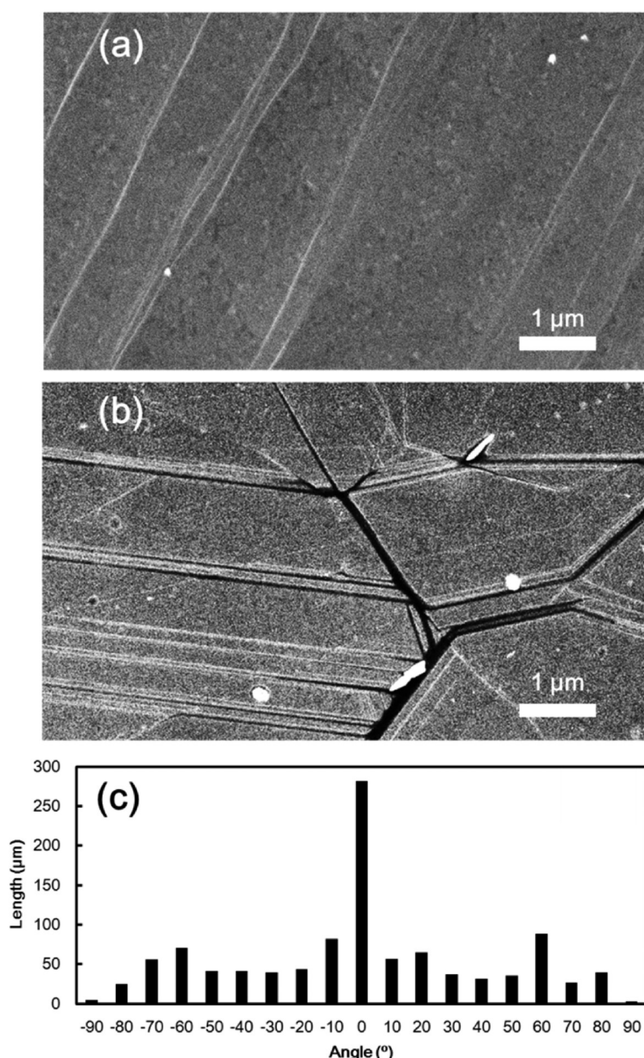

Figure 1. SEM images of the HOPG surface (a) before and (b) after etching in SCW and (c) histogram of integrated trench lengths versus trench angle, where the longest trench in each image was defined as the standard (at 0°).

in SCW, respectively. After SCW treatment (Figure 1(b)), many straight lines, which were not detectable before the SCW treatment (Figure 1(a)), were observed as in previous works on crystallographic etching of graphite/graphene by catalytic particles.[10−15] Using atomic force microscopy (AFM), we confirmed that these lines are trenches (see Supporting Information Figure S2). When SCW treatment was performed without air, no trench was observed on the HOPG. Therefore, crystallographic etching in SCW should be promoted by catalytic carbon oxidation with oxygen dissolved in SCW.

On the other hand, we found that water also contributes to the etching reaction in SCW by varying the water density (see Supporting Information Figure S3). An apparent increase in the etching rate with increasing water density was observed at the water density above 0.1 g/mL. This result indicates that the water contributes to the enhancement of the oxidation reaction. It is reported that during supercritical water oxidation (SCWO), which is the oxidative decomposition in SCW with oxygen, water density effects on the reaction rate can also be observed.[23,24] There are several possible enhancement effects derived from SCW for carbon oxidation, such as the efficient removal of adsorbed gaseous products (CO, CO_2) from the catalyst surface and the formtation of hydroxyl (OH) and hydroperoxyl (HO_2) radicals which are suggested to be dominant reactants in elementary reaction steps in SCWO.[24,25] Although the mechanism for catalytic carbon oxidation in SCW is still not fully understood, the water medium definitely promotes the carbon oxidation in SCW.

Figure 1(c) is a histogram of the integrated lengths of the detectable trenches versus the trench angle from the total area of the obtained SEM images (approximately 3000 μm^2). The longest trench in each image was defined as the standard at 0°. Typically, trenches are formed predominantly along a single direction at 0°, with other relatively preferred directions at ±60°. The existence of these preferred trench directions spaced at 60° intervals strongly supports the hypothesis that the movement of the catalytic nanoparticle reflects the graphene/graphite honeycomb lattice. In a previous study on catalytic carbon gasification, it was verified that the removal of "armchair" carbon atoms is energetically favorable as compared to removal of "zigzag" atoms, and zigzag edges are dominantly introduced.[11,14,15,20] It is thus strongly anticipated that the edges introduced by the SCW treatment in this study are zigzag edges.

In addition to the trenches, folded graphene layers and traces of peeled-off graphene (Figure 2(a) and see Supporting Information Figure S4) were also observed on the HOPG surface in the AFM image. Moreover, suspended graphene fragments are observed in the water after the SCW treatment (Figure 2(b)). Previously, several groups including us have reported SCF has an exfoliation and tearing effect of graphene.[26−28] Until now, various kinds of SCFs, such as supercritical CO_2, NMP (*N*-methyl-2-pyrrolidone), DMF (dimethylformamide), and ethanol have been applied to high-quality, gram-scale processable nanographene production. Dinesh et al. reported the direct conversion of graphite powder to a high yield of graphene sheets in which 90%−95% of the exfoliated sheets are <8 layers thick, 6%−10% of which are monolayers.[26] Although the exfoliation effect of SCW has not been reported, it is highly likely that SCW is also effective for the graphene production by exfoliation from graphite. The AFM images obtained here strongly indicate that the exfoliation of graphene from the HOPG surface has taken place simultaneously with the anisotropic etching during the SCW treatment as shown in Figure 2(c).

The HRTEM images of an exfoliated multilayer graphene are shown in Figure 3. Although an abbreviation-corrected TEM (FEI, Titan80−300) was employed at an accelerating voltage of

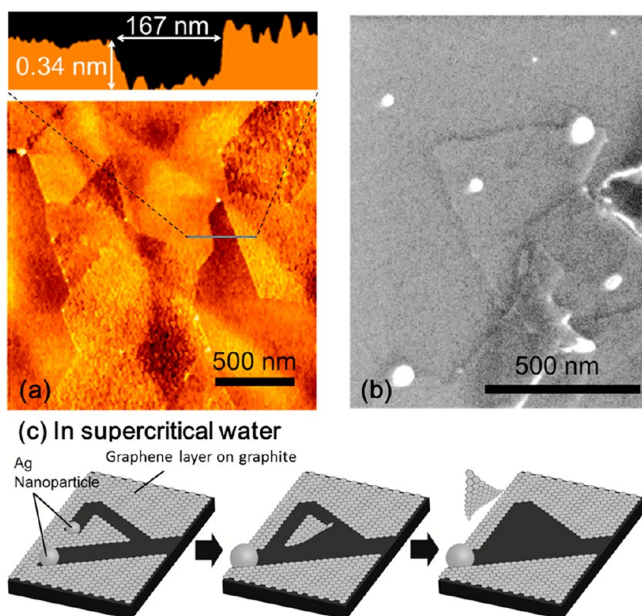

Figure 2. (a) Examples of AFM image containing the traces of graphene peeled off from the HOPG surface, (b) SEM image of graphene fragments suspended in the water after SCF treatment, and (c) scheme of exfoliation of graphene from the graphite surface simultaneously with the anisotropic etching.

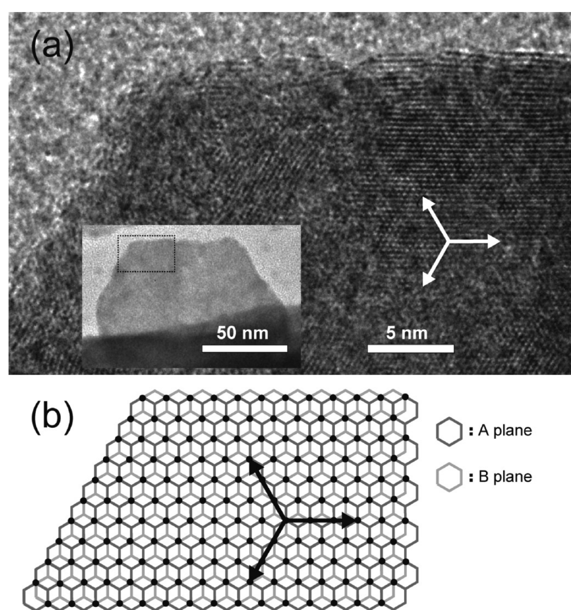

Figure 3. (a) HRTEM image of multilayer graphene fragments suspended in water after SCW treatment (inset is low-magnification TEM image, and the dotted square indicates the area of the HRTEM image). (b) Structural representation of two graphene layers with AB Bernal stacking, where black spots indicate regions of overlapping C atoms. Zigzag directions are indicated by arrows in each figure.

80 kV, the edge structure, which is considered to be more fragile by electroirradiation than the basal plane, has been damaged during the observation. On the other hand, in the basal plane, the clear lattice fringe was obtained. Considering the AB Bernal stacked structure of multilayer graphene as shown in Figure 3(b), the direction of the observed lattice fringe on the graphene in Figure 3(a) should be in parallel with the direction of the zigzag edge. Therefore, it is indicated that the most edges of the multilayer graphene fragment shown in Figure 3(a) consist of zigzag edges and that the anisotropically etched graphene layer on the HOPG was isolated from the HOPG surface. Compared to the previous reports about the exfoliation of graphene using SCF without catalytic nanoparticles, the simultaneous oxidative etching by Ag nanoparticles facilitates the one-step production of anisotropically etched graphene from graphite.

Assuming the trench depth on the HOPG substrate (10 mm × 5 mm) is comparable to the size of the Ag nanoparticles (20−40 nm), the complete exfoliation of the etched layer will provide just a few micrograms of anisotropically etched graphene. To enhance the production yield, the starting graphitic material with large specific surface area, such as graphite powder, is preferable because the etching and the exfoliation progress at the graphite surface. Then, we demonstrated that the etching and the exfoliation are applicable for graphite powder dispersed in SCW. In this case, we mixed 10 mg of ground HOPG powder and the above-mentioned Ag dispersion using a sonication bath and dried it in a vacuum oven at 70 °C. The procedure for the SCW treatment is the same as that for the HOPG substrate. The SEM images of the graphite powder sample and the small fragment sample after the treatment are shown in Figure 4(a) and (b), respectively.

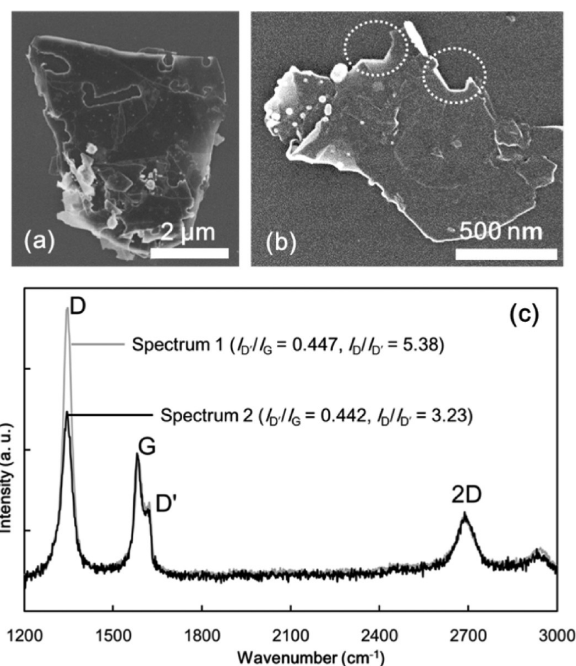

Figure 4. SEM images of (a) graphite powder sample and (b) small fragment sample after SCW treatment with Ag nanoparticle (dotted circle indicates the edges having anisotropically etched geometry) and (c) two characteristic spectra for samples after SCW treatment without (spectrum 1) and with (spectrum 2) the Ag nanoparticle.

We confirmed that the trenches are formed on the surface of the large graphite powder via catalytic carbon oxidation. Moreover, we can observe that some parts of the edge in the small carbon fragment (Figure 4(b)), which is supposed to be formed by the exfoliation from the graphite powder surface, show anisotropically etched geometry. These figures indicate that in the case of graphite powder the exfoliation of graphene has taken place simultaneously with the anisotropic etching during the SCW treatment similar to the HOPG substrate.

To verify the introduction of a zigzag edge to the bulk graphite powder, we conducted a Raman spectroscopic analysis. The two characteristic spectra for graphene/graphite samples obtained in this study are shown in Figure 4(c). These two spectra are almost the same with the exception of the difference of D band intensity. It has been reported that the D band at around 1350 cm^{-1} and the D′ band at around 1620 cm^{-1} can be attributed to defect-induced scattering of graphite, and the graphite edge also behaves as defects. The D band intensity from a zigzag edge is weaker than that from an armchair edge, while the D′ band intensity does not show the dependence on the edge type because of the different intrinsic structural properties of the scattering process for different graphite edges.[29] Here, we discuss the introduction of the zigzag edge by using intensity ratio between the D band and the D′ band ($I_D/I_{D'}$).

Table 1 shows the average $I_D/I_{D'}$ for pristine graphite powder and the samples after SCW treatment with and without Ag nanoparticles. By the SCW treatment without Ag nanoparticles, the slight decrease in the average $I_D/I_{D'}$ was observed. It is supposed that the tearing effect of SCF downsizes the graphite and introduces the additional edges. If the proportion of zigzag edge in the additional edges is larger than that in the pristine graphite powder, it is reasonable that the decrease in the $I_D/I_{D'}$ occurs only by SCW treatment. In the case of the sample after SCW treatment with Ag nanoparticles, the $I_D/I_{D'}$ value was smaller than that in the case without Ag nanoparticles. This result indicates that zigzag edges are introduced by crystallographic etching in SCW even to the dispersed graphite powder. Assuming that the pristine graphite powder has only armchair edge, the proportion of zigzag edge in the sample after crystallographic etching in SCW can be estimated as approximately 20%. It is highly anticipated that the control of etching reaction rate (e.g., by varying etching temperature and oxygen concentration and adding oxidizing agent) enables us to control the proportion of zigzag edge, systematically.

Table 1. Average Intensity Ratio between the D Band and D′ Band ($I_D/I_{D'}$) for Different Powder Samples

	sample	$I_D/I_{D'}$
1	pristine graphite powder	5.0
2	SCW-treated graphite powder without Ag	4.7
3	SCW-treated graphite powder with Ag	4.1

In conclusion, we developed a one-step method for the production of anisotropically etched graphene using SCW. We succeeded in anisotropic oxidative etching of the graphite surface by Ag nanoparticles by the assistance of SCW. It was verified that the crystallographic etching in SCW occurs even for the dispersed powder sample, and graphene, to which the zigzag edges were introduced, was isolated via the exfoliation effect of SCF. Although the etching and the exfoliation progress only on the surface, the employment of graphite powder with large specific surface area as a starting material enhances the production yield of anisotropically etched graphene. This scalable and facile production method for the graphene with controlled edge will facilitate clarification of the preferable edge state of graphene for electrochemical devices and contribute to the enhancements of their performances.

■ ASSOCIATED CONTENT

Supporting Information

SEM images of the HOPG surfaces after the etching by varying temperature (S1); AFM images of the HOPG surface after the etching in SCW (S2); SEM images of the HOPG surfaces after the etching by varying water density (S3); AFM image of folded graphene layers on the HOPG surface after SCW treatment (S4). This material is available free of charge via the Internet at http://pubs.acs.org.

■ AUTHOR INFORMATION

Corresponding Authors

*E-mail: tomai@tagen.tohoku.ac.jp.

*E-mail: i.honma@tagen.tohoku.ac.jp.

Notes

The authors declare no competing financial interest.

■ ACKNOWLEDGMENTS

We thank Dr. Masaru Watanabe and Dr. Taku Aida (Tohoku University) for helpful discussion and Y. Hayasaka and E. Aoyagi (Tohoku University) for TEM observations. This work was financially supported by JSPS KAKENHI Grant Number 24656548.

■ REFERENCES

(1) Son, Y. W.; Cohen, M. M.; Louie, S. G. *Nature* **2006**, *444*, 347.

(2) Enoki, T.; Kobayashi, Y. *J. Mater. Chem.* **2005**, *15*, 3999.

(3) Joly, V. L. J.; Kiguchi, M.; Hao, S.-J.; Takai, K.; Enoki, T.; Sumii, R.; Amemiya, K.; Muramatsu, H.; Hayashi, T.; Kim, Y. A.; Endo, M.; Delgado, J. C.; Urías, F. L.; Méndez, A. B.; Terrones, H.; Terrones, M.; Dresselhaus, M. S. *Phys. Rev. B* **2010**, *81*, 245428.

(4) Tada, K.; Haruyama, J.; Yang, H. X.; Chshiev, M.; Matsui, T.; Fukuyama, H. *Appl. Phys. Lett.* **2011**, *99*, 183111.

(5) Yoo, E.; Okata, T.; Akita, T.; Kohyama, M.; Nakamura, J.; Honma, I. *Nano Lett.* **2009**, *9*, 2255.

(6) Yang, S.; Feng, X.; Zhi, L.; Cao, Q.; Maier, J.; Mullen, K. *Adv. Mater.* **2010**, *22*, 838.

(7) Mitani, S.; Sathish, M.; Rangappa, D.; Unemoto, A.; Tomai, T.; Honma, I. *Electrochim. Acta* **2012**, *68*, 146.

(8) Tomai, T.; kawaguchi, Y.; Sathish, M.; Honma, I. *Electrochim. Acta* **2013**, *92*, 421.

(9) Yumura, T.; Kimura, K.; Kobayashi, H.; Tanaka, R.; Okumura, N.; Yamabe, T. *Phys. Chem. Chem. Phys.* **2009**, *11*, 8275.

(10) Datta, S. S.; Strachan, D. R.; Khamis, S. M.; Johnson, A. T. C. *Nano Lett.* **2008**, *8*, 1912.

(11) Ci, L.; Xu, Z.; Wang, L.; Gao, W.; Ding, F.; Kelly, K. F.; Yakobson, B. I.; Ajayan, P. M. *Nano Res.* **2008**, *1*, 116.

(12) Schäffel, F.; Warner, J. H.; Bachmatiuk, A.; Rellinghaus, B.; Büchner, B.; Schultz, L.; Rümmeli, M. H. *Nano Res.* **2009**, *2*, 695.

(13) Severin, N.; Kirstein, S.; Sokolov, I. M.; Rabe, J. P. *Nano Lett.* **2009**, *9*, 457.

(14) Booth, T. J.; Pizzocchero, F.; Andersen, H.; Hansen, T. W.; Wagner, J. B.; Jinschek, J. R.; Dunin-Borkowski, R. E.; Hansen, O.; Bøggild, P. *Nano Lett.* **2011**, *11*, 2689.

(15) Wang, R.; Wang, J.; Gong, H.; Luo, Z.; Zhan, D.; Shen, Z.; Thong, J. T. L. *Small* **2012**, *8*, 2515.

(16) Sharma, R.; Nair, N.; Strano, M. S. *J. Phys. Chem. C* **2009**, *113*, 14771.

(17) Jiang, D. S.; Sumpter, B. G.; Dai, S. *J. Chem. Phys.* **2007**, *126*, 134701.

(18) Koskinen, P.; Malola, S.; Häkkinen, H. *Phys. Rev. Lett.* **2008**, *101*, 115502.

(19) Harris, P. S.; Feates, F. S.; Reuben, B. G. *Carbon* **1974**, *12*, 189.

(20) Goethel, P. J.; Yang, R. T. *J. Catal.* **1989**, *119*, 201.

(21) Pan, Z. J.; Yang, R. T. *J. Catal.* **1991**, *130*, 161.

(22) Chen, S. G.; Yang, R. T. *J. Catal.* **1992**, *138*, 12.

(23) Koo, M.; Lee, W. K.; Lee, C. H. *Chem. Eng. Sci.* **1997**, *52*, 1201.
(24) Holgate, H. R.; Tester, J. W. *J. Phys. Chem.* **1994**, *98*, 810.
(25) Brock, E. E.; Oshima, Y.; Savage, P. E.; Barker, J. R. *J. Phys. Chem.* **1996**, *100*, 15834.
(26) Rangappa, D.; Sone, K.; Wang, M.; Gautam, U. K.; Golberg, D.; Itoh, H.; Ichihara, M.; Honma, I. *Chem.—Eur. J.* **2010**, *16*, 6488.
(27) Pu, N.; Wang, C.; Sung, Y.; Liu, Y.; Ger, M. *Mater. Lett.* **2009**, *63*, 1987.
(28) Tomai, T.; Kawaguchi, Y.; Honma, I. *Appl. Phys. Lett.* **2012**, *100*, 233110.
(29) Cancado, L. G.; Pimenta, M. A.; Neves, B. R. A.; Dantas, M. S. S.; Jorio, A. *Phys. Rev. Lett.* **2004**, *93*, 247401.